

TrackerBots: Autonomous UAV for Real-Time Localization and Tracking of Multiple Radio-Tagged Animals

Hoa Van Nguyen

School of Computer Science
The University of Adelaide
SA 5005, Australia

hoavan.nguyen@adelaide.edu.au

Michael Chesser

School of Computer Science
The University of Adelaide
SA 5005, Australia

michael.chess@adelaide.edu.au

Lian Pin Koh

School of Ecology and Environmental Science
The University of Adelaide
SA 5005, Australia

lianpin.koh@adelaide.edu.au

S. Hamid RezaTofighi

School of Computer Science
The University of Adelaide
SA 5005, Australia

hamid.rezatofighi@adelaide.edu.au

Damith C. Ranasinghe

School of Computer Science
The University of Adelaide
SA 5005, Australia

damith.ranasinghe@adelaide.edu.au

Abstract

Autonomous aerial robots provide new possibilities to study the habitats and behaviors of endangered species through the efficient gathering of location information at temporal and spatial granularities not possible with traditional manual survey methods. We present a novel autonomous aerial vehicle system—*TrackerBots*—to track and localize multiple radio-tagged animals. The simplicity of measuring the received signal strength indicator (RSSI) values of very high frequency (VHF) radio-collars commonly used in the field is exploited to realize a low cost and lightweight tracking platform suitable for integration with unmanned aerial vehicles (UAVs). Due to uncertainty and the nonlinearity of the system based on RSSI measurements, our tracking and planning approaches integrate a particle filter for tracking and localizing; a partially observable Markov decision process (POMDP) for dynamic path planning. This approach allows autonomous navigation of a UAV in a direction of maximum information gain to locate multiple mobile animals and reduce exploration time; and, consequently, conserve on-board battery power. We also employ the concept of a search termination criteria to maximize the number of located animals within power constraints of the aerial system. We validated our real-time and online approach through both extensive simulations and field experiments with two mobile VHF radio-tags.

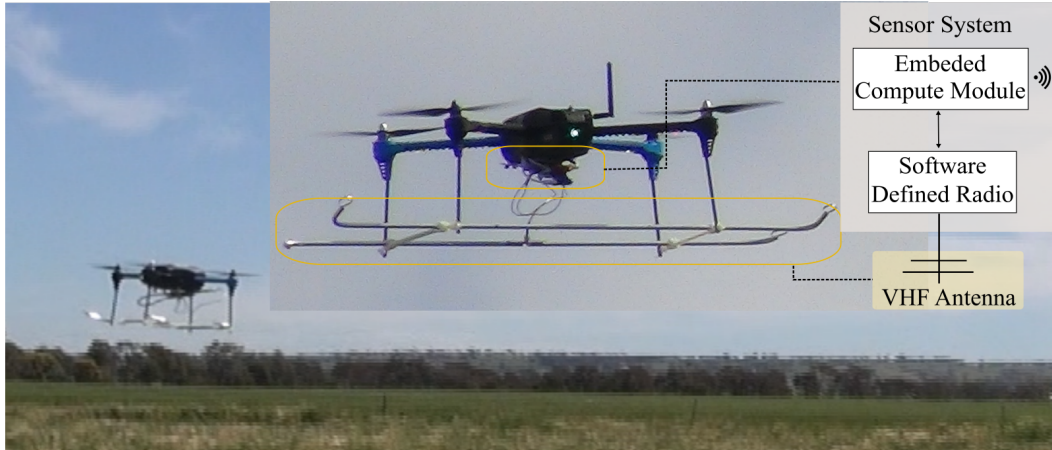


Figure 1: *TrackerBots*: An overview of the UAV tracking platform with its sensor system.

1 Introduction

Understanding basic questions of ecology such as how animals use their habitat, their movements and activities are necessary for addressing numerous environmental challenges ranging from invasive species to diseases spread by animals and saving endangered species from extinction. Conservation biologists, ecologists as well as natural resource management agencies around the world rely on numerous methods to monitor animals. Today, capturing and collaring concerned species with Very High Frequency (VHF) radio tags and the subsequent use of VHF telemetry or radio tracking is the most important and cost effective tool employed to study the movement of a wide range of animal sizes (Wikelski et al., 2007) in their natural environments (Kays et al., 2011; Thomas et al., 2012).

However, the traditional method of radio tracking typically requires researchers to trek long distances in the field, armed with cumbersome VHF radio receivers with hand-held antennas and battery packs to manually home in on radio signals emitted from radio-tagged or collared animals. Consequently, the precious spatial data acquired through radio tracking comes at a significant cost to researchers in terms of manpower, time and funding. The problem is often compounded by other challenges, such as low animal recapture rates, equipment failures, and the inability to track animals that move into inaccessible terrain. Furthermore, many of our most endangered species also happen to be the most difficult to track due to their small size, inconspicuousness, and location in remote habitats.

Automated tracking and location of wildlife with autonomous unmanned aerial vehicles (UAVs) can provide *new* possibilities to better understand ecology and our native wildlife to safeguard biodiversity and manage our natural resources cost-effectively. We present a low-cost approach capable of realization in a lightweight payload for transforming existing commodity drone platforms into autonomous aerial vehicle systems as shown in Fig. 1 to empower conservation biologists to track and localize multiple radio-tagged animals.

The main contribution of our work is a new autonomous aerial vehicle system for simultaneously tracking and localizing multiple mobile radio-tagged animals using VHF radio-collars, commonly used in the field. In particular:

- Our system is realized in a 260 g payload suitable for a multitude of low-cost, versatile, easy to operate multi-rotor UAVs without a remote pilot license. Our lightweight realization—of less than 2 kg system mass—is achieved through a new sensor design that exploits the simplicity of a software defined radio architecture for capturing received signal strength indicator (RSSI) value from multiple VHF radio tags and a compact, lightweight VHF antenna geometry.
- We formulate a *joint* tracking and path planning problem to realize a real-time and online autonomous system. Due to the noisy, complex and nonlinear characteristics of RSSI data we integrate a sequential Monte Carlo implementation of a Bayesian filter, also known as particle filter (PF), for real-time tracking and localization

jointly with a partially observable Markov decision process (POMDP) with Rényi divergence between prior and posterior estimates of animal locations for autonomy and dynamic online path planning to minimize flight time while maximizing number of located animals. Further, our formulation considers the trade-off between location accuracy and resource constraints of the UAV, its maneuverability, and power constraints to develop a practical solution.

- We validate our method through extensive simulations and field experiments with mobile VHF radio-tags.
- In order to support researchers in the field and facilitate adoption of new technologies in the field, we provide a complete design description of *TrackerBots*, including a repository of source code to develop our fully autonomous system ¹

2 Related Work

Since this application is related to locating VHF collared animals, we will focus on progress made towards the autonomous localization and tracking of multiple VHF radio-tagged animals here.

Off-line estimations of a radio beacon from data logged from a UAV have been demonstrated in (Jensen et al., 2014; Wagle and Frew, 2011). Pioneering achievements in autonomous wildlife tracking have been made through simulation studies (Posch and Sukkarieh, 2009) and experimentally demonstrated systems (Cliff et al., 2015; Körner et al., 2010; Tokekar et al., 2010; Vander Hook et al., 2014) in recent years. In particular, the first demonstration of a UAV was presented in (Cliff et al., 2015).

The recent approaches (Cliff et al., 2015; Vander Hook et al., 2014) for real-time localization of a static target (assuming stationary wildlife) used wireless signal characteristics captured by a narrowband receiver to estimate location; in particular, the angle-of-arrival (AoA) of a radio beacon was determined using an array of antennas with the information related to a ground-based receiver for location estimations. Although the approach can conveniently manage topological variations in terrain, AoA systems require a large bulky receiver system and multiple antenna elements as well as long observation times; 45 seconds per observation as reported in (Cliff et al., 2015). Moreover, the antenna systems being mounted on top of the UAV (Cliff et al., 2015) is likely to lead to difficulty in tracking terrestrial animals although being suitable for locating avian species dwelling in trees.

We can see that there are few investigations that have studied the problem of locating radio-collared animals using autonomous robots. Although a system based on angle-of-arrival was recently evaluated to locate a stationary animal, the development of a low-cost and lightweight autonomous system capable of long-range flights and localization of multiple *mobile* radio-collared animals still remains. This is especially significant in the realization of a system that is widely accessible to conservation biologists in the field where a very small UAV—of less than 2 kg—can be flown without a formal pilot license and with fewer restrictions given the exclusion of this category of UAVs from regulatory regimes (Civil Aviation Safety Authority, 2017)

We present an alternative approach exploiting RSSI based range only measurements because of the ability to use a simpler sensing system on board commodity UAVs to realize lower cost and longer flight range UAVs for tracking and localizing multiple animals. Together with a strongly principled approach for joint tracking and planning, our lightweight autonomous aerial robot platform provides a cost-effective method for wildlife conservation and management.

¹see: <https://github.com/AdelaideAuto-IDLab/TrackerBots> (please note that project material will be fully uploaded upon the acceptance of the article for publication)

3 Tracking and Planning Problem Formulation

Real-time tracking requires an online estimator and a dynamic planning method. This section presents our tracking and localizing formulation under a principled framework of a Bayesian filter for tracking and POMDP for planning strategy.

3.1 Tracking and localizing

For tracking, we use a Bayesian filter. It is an online estimation technique which deals with the problem of inferring knowledge about the unobserved state of a dynamic system—in our problem, wildlife—which changes over time, from a sequence of noisy measurements. Suppose $\mathbf{x} \in \mathcal{X}$ and $\mathbf{z} \in \mathcal{Z}$ are respectively the system (kinematic) state vector in the state space \mathcal{X} and the measurement (observation) vector in the observation space \mathcal{Z} . The problem is estimating the state $\mathbf{x} \in \mathcal{X}$ from the measurement $\mathbf{z} \in \mathcal{Z}$ or calculating the marginal posterior distribution $p(\mathbf{x}_k | \mathbf{z}_{1:k})$ sequentially through *prediction* (1) and *update* (2) steps.

$$p(\mathbf{x}_k | \mathbf{z}_{1:k-1}) = \int p(\mathbf{x}_k | \mathbf{x}_{k-1}) p(\mathbf{x}_{k-1} | \mathbf{z}_{1:k-1}) d\mathbf{x}_{k-1} \quad (1)$$

$$p(\mathbf{x}_k | \mathbf{z}_{1:k}) = \frac{p(\mathbf{z}_k | \mathbf{x}_k) p(\mathbf{x}_k | \mathbf{z}_{1:k-1})}{\int p(\mathbf{z}_k | \mathbf{x}_k) p(\mathbf{x}_k | \mathbf{z}_{1:k-1}) d\mathbf{x}_k} \quad (2)$$

In the case of a nonlinear system or non-Gaussian noise, there is no general closed-form solution for the Bayesian recursion and $p(\mathbf{x}_k | \mathbf{z}_{1:k})$ generally has a non-parametric form. Therefore, in our problem, we use a particle filter implementation as an approximate solution for the Bayesian filtering problem due to our highly nonlinear measurement model.

Particle Filter (PF): A particle filter uses a sampling approach to represent the non-parametric form of the posterior density $p(\mathbf{x}_k | \mathbf{z}_{1:k})$. The samples from the distribution are represented by a set of particles; each particle has a weight assigned to represent the probability of that particle being sampled from the probability density function. Then, these particles representing the nonparametric form of $p(\mathbf{x}_k | \mathbf{z}_{1:k})$ are propagated over time. In the simplest version of the particle filter, known as the bootstrap filter first introduced by Gordon in (Gordon et al., 1993), the samples are directly generated from the transitional dynamic model. Then, to reduce the particle degeneracy, resampling and injection techniques are implemented; a detailed algorithm can be found in (Ristic et al., 2004).

Measurement model: The update process of a PF requires the derivation of a likelihood of measurements. In our problem, based on estimating a target's—VHF radio tag's—range from the receiver, we require a realistic signal propagation model to obtain the likelihood of receiving a given measurement. We employ two VHF signal propagation models suitable for describing RSSI measurements in non-urban outdoor environments (Patwari et al., 2005; Jakes, 1974). Denoting $\mathbf{h}(\mathbf{x}, \mathbf{u})$ as the RSSI measurement function between target \mathbf{x} and observer (UAV) state \mathbf{u} , we have:

i) Log Distance Path Loss Model (LogPath): The received power is the only line of sight power component transmitted from a transmitter subjected to signal attenuation such as through absorption and propagation loss (Patwari et al., 2005):

$$\mathbf{h}(\mathbf{x}, \mathbf{u}) = P_r^{d_0} - 10n \log_{10}(d(\mathbf{x}, \mathbf{u}_p)/d_0) + G_r(\mathbf{x}, \mathbf{u}) \quad (3)$$

where

- $\mathbf{x} = [p_x^t, p_y^t, p_z^t]^T$ is the target's position; $\mathbf{u}_p = [p_x^u, p_y^u, p_z^u]^T$ is the observer's (UAV) position in Cartesian coordinates; $\mathbf{u} = [\mathbf{u}_p; \theta^u]$ is the UAV's state which includes its heading angle θ^u .

- $d(\mathbf{x}, \mathbf{u}_p)$ is the euclidean distance between the target's position and UAV's position.
- $G_r(\mathbf{x}, \mathbf{u})$ is the UAV receiver antenna gain which depends on its heading, its position, and target's position (details explained in Sec. 6.2).
- $P_r^{d_0}$ is received power at a reference distance d_0 .
- n is the path-loss exponent that characterizes the signal losses such as absorption and propagation losses and this parameter depends on the environment with typical values ranging from 2 to 4 (Patwari et al., 2005).

ii) Log Distance Path Loss Model with Multi-Path Fading (MultiPath): The received power is composed of both line of sight power component transmitted from a transmitter and the multi-path power component reflected from the ground plane subjected to signal attenuation such as through absorption and propagation loss: (Jakes, 1974, p. 81):

$$\begin{aligned} \mathbf{h}(\mathbf{x}, \mathbf{u}) = & P_r^{d_0} - 10n \log_{10}(d(\mathbf{x}, \mathbf{u}_p)/d_0) \\ & + G_r(\mathbf{x}, \mathbf{u}) + 10n \log_{10}(|1 + \Gamma(\psi)e^{-j\Delta\varphi}|) \end{aligned} \quad (4)$$

where, in addition to terms in 3

- ψ is the angle of incidence between the reflected path and the ground plane.
- $\Gamma(\psi) = [\sin(\psi) - \sqrt{\varepsilon_g - \cos^2(\psi)}] / [\sin(\psi) + \sqrt{\varepsilon_g - \cos^2(\psi)}]$ is the ground reflection coefficient with ε_g is the relative permittivity of the ground.
- $\Delta\varphi = 2\pi\Delta d/\lambda$ is the phase difference between two waves where λ is the wave length and $\Delta d = ((p_x^t - p_x^u)^2 + (p_y^t - p_y^u)^2 + (p_z^t + p_z^u)^2)^{1/2} - d(\mathbf{x}, \mathbf{u})$.

In non-urban environments, received power is usually corrupted by environmental noise, with the assumption that the noise is white, the total received power $\mathbf{z} = P_r(\mathbf{x}, \mathbf{u})$ [dBm] is:

$$\mathbf{z} = \mathbf{h}(\mathbf{x}, \mathbf{u}) + \eta_P \quad (5)$$

where $\eta_P \sim \mathcal{N}(0, \sigma_P^2)$ is Gaussian white noise with covariance σ_P^2 . Notably, even if RSSI noise is not completely characterized by a white noise model, we found it practical to characterize the received noise with a white Gaussian model as shown in Fig. 7.

We use data captured in experiments using our sensor system to validate the physical sensor characteristics $G_r(\mathbf{x}, \mathbf{u})$ (see Sec. 4) and n defined by environmental characteristics, as well as estimate the propagation model reference power parameter $P_r^{d_0}$ and noise σ_P (see Sec. 6.2).

Measurement likelihood: Based on (5) with Gaussian noise η_P , the likelihood of measurement \mathbf{z}_k , given target and sensor position are \mathbf{x}_k and \mathbf{u}_k , respectively, at time k is

$$p(\mathbf{z}_k | \mathbf{x}_k, \mathbf{u}_k) \sim \mathcal{N}(\mathbf{z}_k; \mathbf{h}(\mathbf{x}_k, \mathbf{u}_k), \sigma_P^2) \quad (6)$$

where $\mathcal{N}(\cdot; \mu, \sigma^2)$ is a normal distribution with mean μ and covariance σ^2 .

3.2 Path Planning

The UAV planning problem is similar to the problem of an agent computing optimal actions under partially observable Markov decision process (POMDP) to maximize its reward. (Kaelbling et al., 1998) have shown that a POMDP framework implements an efficient and *optimal* approach based on previous actions and observations to determine the

true world states. POMDP in conjunction with a particle filter provides a principled approach for evaluating planning decision to realize an autonomous system for tracking.

In general, a POMDP is described by the 6-tuple $(\mathcal{S}, \mathcal{A}, \mathcal{T}, \mathcal{R}, \mathcal{O}, \mathcal{Z})$ where \mathcal{S} is set of both UAV and target states ($\mathbf{s} = \{\mathbf{x}, \mathbf{u}\} \in \mathcal{S}$), \mathcal{A} is set of UAV actions, \mathcal{T} is state-transition function $\mathcal{T}(\mathbf{s}, \mathbf{a}, \mathbf{s}') = p(\mathbf{s}'|\mathbf{s}, \mathbf{a})$ for a given action \mathbf{a} , $\mathcal{R}(\mathbf{a})$ is reward function, \mathcal{O} is set of observations and \mathcal{Z} is observation likelihood $\mathcal{Z}(\mathbf{s}, \mathbf{a}, \mathbf{o}) = p(\mathbf{o}|\mathbf{s}, \mathbf{a})$ with $\mathbf{s}, \mathbf{s}' \in \mathcal{S}$ is current state and next state respectively, $\mathbf{a} \in \mathcal{A}$ is taken action and $\mathbf{o} \in \mathcal{O}$ is the observation—i.e measurement. The goal of a POMDP is to find an optimal policy to maximize the total expected reward $\mathbb{E}[\sum_{\kappa=k}^{k+H} \gamma^{\kappa-k} \mathcal{R}_{\kappa}(\mathbf{a}_k)]$ where H is look-ahead horizon steps, γ is the discount factor which serves as the value difference between the current reward versus the future reward; \mathbf{a}_k is action at time step k and $\mathbb{E}[\cdot]$ is the expectation operator (Hsu et al., 2008).

The reward function can be calculated using different methods such as task-driven or information-driven strategies. When uncertainty is high, the information gain approach is preferable to reduce a target's location uncertainty (Beard et al., 2017); hence, we used this method to calculate our reward function. There are several approaches to evaluate information gain in robotic path planning such as Shannon entropy (Cliff et al., 2015), Kullback-Leibler (KL) divergence or Rényi divergence (Hero et al., 2008). We adapted the approach in (Ristic, 2013; Ristic and Vo, 2010) to implement Rényi divergence as our reward function since it fits naturally with our Monte-Carlo sampling method. Here, Rényi divergence measures the information gain between prior and posterior densities (Beard et al., 2017; Ristic and Vo, 2010):

$$\mathcal{R}_{k+H}^{(i)}(\mathbf{a}_k) = \frac{1}{\alpha - 1} \log \int [p(\mathbf{x}_{k+H}|\mathbf{z}_{1:k})]^\alpha \times [p(\mathbf{x}_{k+H}|\mathbf{z}_{1:k}, \mathbf{z}_{k+1:k+H}^{(i)}(\mathbf{a}_k))]^{1-\alpha} d\mathbf{x}_{k+H}, \quad (7)$$

where $\alpha \geq 0$ is a scale factor to decide the effect from the tails of two distributions. The prior density $p(\mathbf{x}_{k+H}|\mathbf{z}_{1:k})$ is calculated by propagating current posterior particles sampled from $p(\mathbf{x}_k|\mathbf{z}_{1:k})$ to time $k + H$ using the prediction step (1). The posterior density $p(\mathbf{x}_{k+H}|\mathbf{z}_{1:k}, \mathbf{z}_{k+1:k+H}^{(m)}(\mathbf{a}_k))$ where $\mathbf{z}_{k+1:k+H}^{(m)}(\mathbf{a}_k)$ is the *future* measurement set that will be observed if action $\mathbf{a}_k \in \mathcal{A}_k$ is taken; this is calculated by applying both prediction (1) and update steps (2) up to time $k + H$. However, using Bayes update procedure is computationally expensive and prohibitive in a real-time setting. Instead, we implement a computationally efficient approach using a black box simulator proposed in (Silver and Veness, 2010) along with the Monte Carlo sampling approach. Hence, the problem transforms to find an optimal action $\mathbf{a}_k^* \in \mathcal{A}_k$ to maximize total expected reward:

$$\mathbf{a}_k^* \approx \arg \max_{\mathbf{a}_k \in \mathcal{A}_k} \frac{1}{M_s} \sum_{t=k}^{k+H} \sum_{m=1}^{M_s} \gamma^{t-k} \mathcal{R}_t^{(m)}(\mathbf{a}_k), \quad (8)$$

where M_s is the number of future measurements.

3.3 Multi-targets Tracking

The particle filter proposed in Sec. 3.1 can be extended to multi-target tracking (MTT). However, MTT normally deals with the complex data association problem where it is difficult to determine which measurement belongs to which target. In contrast, for our system, each target can be estimated from the measurement based on the signal frequency and tracked independently. Thus, we do not need to solve the data association problem. Notably, not all of the targets are detected due to, for example, the UAV movements, the measurement range limits imposed by propagations losses and receiver sensitivity. Therefore, if the target is not detected, the solver does not update its estimated position.

Besides maximizing the number of targets localized and tracked, we formulated a termination condition for each target to conserve UAV battery power; a target is considered localized if its location uncertainty, determined by a determinant of its particles covariance, is sufficiently small ($< N_{Th}$). Then, those found targets are *forgotten* to aid the solver to prioritize its computing resources on those targets with high uncertainty.

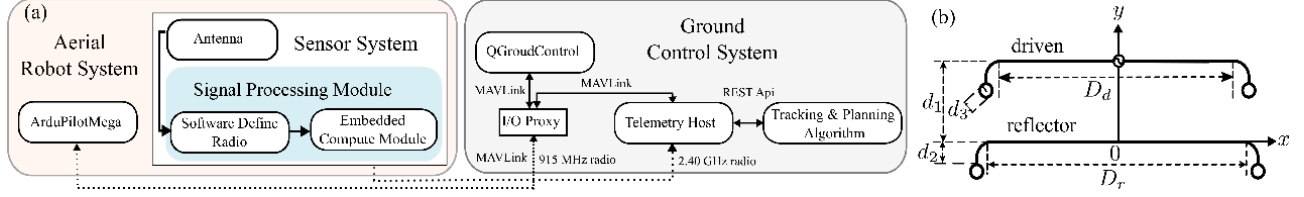


Figure 2: a) The full communication channels between UAV and the ground control system with its main software components and protocols. b) The folded 2-element Yagi antenna design used in our sensor system for observations.

4 System Implementation

We implemented an experimental aerial robot system based on our tracking and planning formulation. An overview of the complete system is described in Fig. 2a. Our experimental system used a 3DR IRIS+ UAV platform and a new sensor system built with: i) a compact directional VHF antenna design, and ii) a software-defined signal processing module capable of simultaneously processing signals from multiple targets and remotely communicate with a ground control system for tracking and planning. In our system, the ArduPilotMega (APM) on the IRIS+ UAV transmits back its global positioning system (GPS) location to the Telemetry Host tool developed by our group to communicate with the APM module using the MAVLink protocol over a 915 MHz full duplex radio channel. The sensor system together with the Antenna, SDR receiver, and the embedded compute module delivers targets’ RSSI data through a 2.40 GHz radio channel to the ground control system.

GPS location of the UAV platform and targets’ RSSI data are delivered to our tracking and planning algorithm—*solver*—through the Telemetry Host using a RESTful web service. The solver estimates target locations and calculates new control actions per each POMDP cycle to command the UAV through MAVLink to fly to a new location. In order to ensure safety and meet University regulatory requirements, we also employ QGroundControl—a popular cross-platform flight control and mission planning software—to monitor and abort autonomous navigation. We detail our Sensor System below.

Signal Processing Module: Fig. 3 illustrates the components of the proposed signal processing module. We propose using a *software defined radio* (SDR) receiver to implement the signal processing components. The key advantages of our choice are the ability to: i) reduce the weight of the receiver; ii) rapidly scan a large frequency spectrum to track multiple animals beaconing on different VHF frequency channels; and iii) because the signal processing chain is defined in software, we have the ability to reconfigure the system on the fly.

In this work, we use the *HackRF One* SDR—an open source platform developed by (Ossmann, 2015) capable of directly converting radio frequency (RF) signals to digital signals using an analog-to-digital converter (ADC)—together with an Intel Edison board as our embedded compute module. We implemented a Discrete Fourier Transform (DFT) filter to isolate, from multiple signals, each unique VHF frequency channel associated with an animal radio collar and measure the signal strength of the received signal.

Antenna: A lightweight folded 2-element Yagi antenna was specially designed for our sensor system. Our design achieves a low profile antenna capable of being within the form factor of low-cost commodity UAVs suitable for easy operation in the field. Similar to a standard 2-element Yagi antenna, the folded design has one reflector and one driven element as shown in Fig. 2b.

The antenna operates in the frequency range from 145 to 155 MHz (a typical range for wildlife radio tags), and a center frequency of $f = 150$ MHz. The length of driven and reflector elements are $D_d = 0.3975\lambda$ and $D_r = 0.402\lambda$, respectively, while $d_1 = 0.1\lambda$, $d_2 = 0.03\lambda$ and the inductive loading ring diameter is $d_3 = 0.015\lambda$. Here, the wavelength $\lambda = c/f = 2$ (m) with $c = 3 \cdot 10^8$ (m/s). The antenna gain model calculated for the design is shown in Fig. 6b.

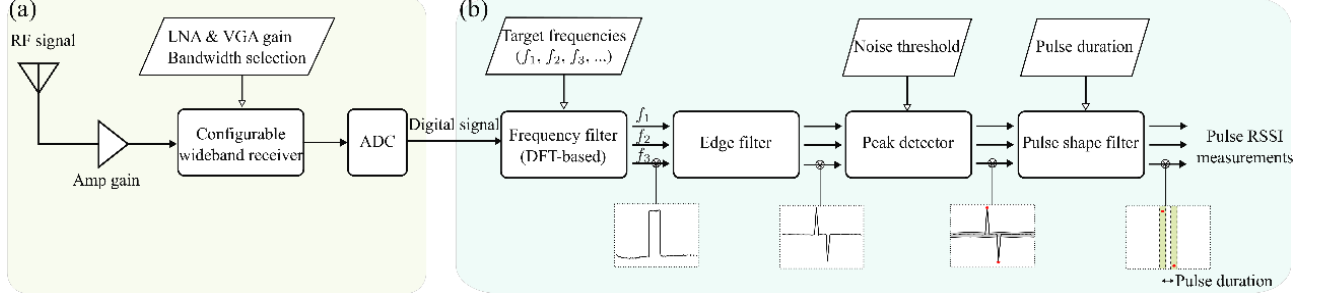


Figure 3: A signal processing module. (a) *Software defined radio*: raw input RF signals go through the HackRF SDR device with different configurable amplifiers - Low Noise Amplifier (LNA) and Variable Gain Amplifier (VGA), and an ADC to convert to digital signals. (b) *Embedded compute module*: digital signals processed on an Edison board using a DFT-based frequency filter with configurable input frequencies, edge filter and peak detector algorithms to derive pulse RSSI measurements.

4.1 Planning implementation for a real-time system

Implementing planning algorithms on any real-time systems is always challenging because of its high computational demand. Thus, in this following, we present the approaches to minimize the planning computational time while not scarifying the overall localization performance:

1. Notably, for RSSI data, the uncertainty in the estimation of a target's location is reduced when the maximum gain of the directional antenna mounted on the UAV points toward the target position. Hence, to increase the localization accuracy, the UAV heading angle θ_k^u must be controlled during the path planning process, although the multi-rotor UAV can be maneuvered without changing its heading. We select a set of discrete UAV rotation angles for the control actions \mathcal{A}_k based on a simulation based study to reduce the computational complexity of the POMDP planning process by limiting the number of possible actions to evaluate.
2. The solver performs planning in every N_p observation cycles with $N_p > 1$ instead of every observation. This approach helps to ensure that the solver prioritizes its limited computational resource on tracking targets instead of only performing planning steps.
3. A coarse planning interval t_p in the planning procedure is implemented to minimize the computational time by reducing the number of look-ahead steps while still having the same look-ahead horizon. For example, we want to estimate the target's state in a 10 second horizon, we can use the normal interval $t_p = 1(s)$ and estimate the target's state 10 times or use the coarser interval $t_p = 5(s)$ and perform the estimation twice; the latter approach is computationally less expensive.
4. Instead of selecting the best action from the possible action space \mathcal{A}_k , the domain knowledge of the receiver antenna gain is used to select a subset of actions that give the highest received gain using **Alg. 1**.

Algorithm 1 Calculate the control action subset

Input: Number of preferred actions $N_{\mathcal{A},s}$, \mathcal{A}_k , the antenna gain G_r , the target's position \mathbf{x}_{k+H}

Output: \mathcal{A}_k^s

- 1: **for** $l = 1 : N_{\mathcal{A},k}$ **do**
 - 2: Get $\mathbf{u}_{k+H}^l \in \mathcal{A}_k(l)$
 - 3: Calculate $G_r^l = G_r(\mathbf{x}_{k+H}, \mathbf{u}_{k+H}^l)$
 - 4: **end for**
 - 5: $\mathcal{A}_k^s = \mathcal{A}_k(G_r^l \geq \text{Top } N_{\mathcal{A},s} \text{ of } G_r)$
-

Following the above implementation approach, UAV motion includes two modes: i) changing its heading angle while hovering; and ii) moving forward to its direct location. In one planning procedure with N_p cycles, the UAV needs $\lfloor |\Delta\theta|/\theta_{max} \rfloor$ cycles to rotate, and spends the remaining cycles $N_p - \lfloor |\Delta\theta|/\theta_{max} \rfloor$ to move forward without changing its heading. Here $\lfloor \cdot \rfloor$ and $|\cdot|$ are the floor and absolute operator respectively, and θ_{max} is the UAV maximum rotation angle in one cycle. The sign of $\Delta\theta$ decides the rotation direction (+ for the clockwise, and – for the counter-clockwise).

5 Simulation Experiments

Implementing on a real system is time-consuming and difficult. Hence, we want to validate our systems first through several simulation experiments to: *i*) verify our tracking and planning algorithms; *ii*) investigate how our planning parameters such as different α values of the Rényi divergence or number of discrete actions $N_{A,s} = |\mathcal{A}_k^s|$ created in Alg. 1 contribute to the overall algorithm performance; and *iii*) compare our proposed Rényi divergence based planning technique with other well-known methods, and the impact of the look-ahead horizon parameters on computational time and localization accuracy. All of the simulation experiments were processed on a PC with an Intel(R) Core(TM) i7-6700 CPU @ 3.40GHz, 32GB RAM and MATLAB-2016b.

5.1 Tracking and Planning Simulation

This simulation was implemented to validate our approach under a synthetic scenario where all parameters (*e.g.* velocity of the UAV v_u) are set to those expected in practice. In this experiment, the UAV attempted to search and localize 10 moving targets randomly located in an area of 500 m \times 500 m. The following are list of parameters used in this simulation: the sampling time step is 1 second since the tag emits pulse signals every 1 second. The solver performed a planning procedure every $N_p = 5$ s, and the look-ahead horizon parameters: $H = N_H t_p = 5$ s with number of horizon $N_H = 1$ and the planning interval $t_p = 5$ s. The UAV started from its home location at $u_1 = [0, 0, 20, 0]^T$, moved under the constant velocity $v_u = 5$ m/s with its maximum heading rotation angle $\theta_{max} = \pi/6$ rad/s. Number of particles for each target were capped at $N_s = 10,000$, with the future sample measurement $M_s = 50$, Rényi divergence parameter $\alpha = 0.5$, number of actions $N_{A,s} = 5$. In addition, a target is considered localized if its location uncertainty, determined by the determinant of its particles covariance, is small enough— $N_{Th} = 10,000 \text{ m}^{2N_s}$ was chosen as the limit. The *LogPath* measurement model with $P_r^{d0} = 7.7$ dBm, $n = 3.1$, $\sigma_P = 4.22$ dB was used to verify our proposed algorithm. To demonstrate that our algorithm was able to localize mobile targets, a *wombat*—an animal that usually wanders around its area was considered. Hence, a *random walk* model was used to describe its behavior with a single target's transitional density:

$$p(\mathbf{x}_k|\mathbf{x}_{k-1}) = \mathcal{N}(\mathbf{x}_k; \mathbf{F}\mathbf{x}_{k-1}, \mathcal{Q}) \quad (9)$$

where $F = \mathbf{I}_3$ with \mathbf{I}_n is $n \times n$ identity matrix, $\mathcal{Q} = \sigma_Q^2 \text{diag}([1, 1, 0]^T)$, $\sigma_Q = 2$ m/s.

Fig. 4 shows localization results for 10 mobile targets where the estimation details are annotated next to the target's position with two indicators: *RMS* and *flight time*—see Sec. 5.2 for definitions. In summary, for this scenario, it took the UAV **587** seconds to localize all ten moving targets a the maximum error distance less than 15 m, except for the outlier, target #2 (RMS = 26.3 m). At flight time 587 s, after finishing localizing the last target (target #7), the UAV was sent a command to fly back to its original station. In this case, the total UAV travel distance was 1.93 km. The results demonstrate that our algorithm can search and accurately localize multiple numbers of targets in real time (about 10 minutes) at the travel distance 1.93 km well within the capacity of commercial off the shelf drones under the 2 kg mass category.

5.2 Monte Carlo simulations

For this experiment, all of Monte Carlo setup parameters were kept the same as in Sec. 5.1, except for those under investigation. In addition, to ensure that the results were not random, all of the conducted experiments were performed

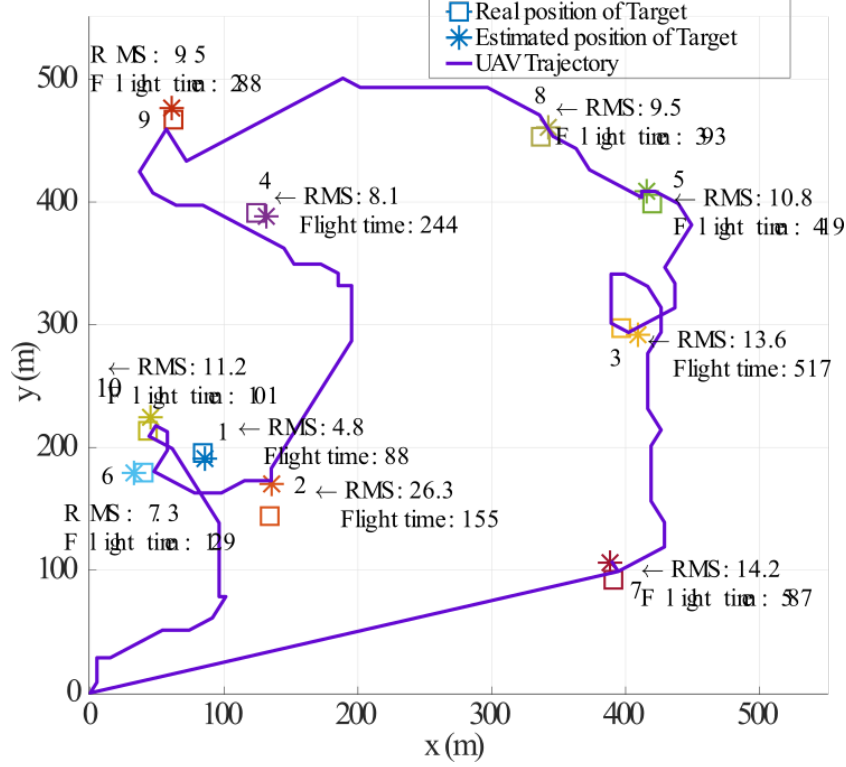


Figure 4: Simulation results with 10 mobile targets localized using a single UAV by Particle Filter and POMDP.

over 100 Monte Carlo runs. The tracking algorithm was evaluated based on the following criterion:

- *Estimation Error* is the absolute distance between ground truth and estimated target location $\mathcal{D}_{rms} = \sum_{j=1}^{N_{tg}} d_{rms}^j / N_{tg}$ with $d_{rms}^j = [(x_{truth}^j - x_{est}^j)^2 + (y_{truth}^j - y_{est}^j)^2]^{1/2}$.
- *Flight time* (s) for UAV to localize **all** of the targets which includes hovering time when the UAV waits for commands from the solver to take an action.
- *UAV travel distance*: the total distance traveled by the UAV to track and locate all of the targets to the required location uncertainty bound; i.e the determinant of covariance being adequately small— $N_{Th} \leq 10,000 \text{ m}^{2N_s}$.
- *Computational cost*: We evaluate the computational cost in terms of two components: i) execution time for the solver to execute the tracking algorithm only (called *non-planning time*), and ii) the execution time for the solver to select the best action—planning step—as well as complete the tracking task (called *planning time*).

First, our search and localization algorithms were evaluated using different α values for Rényi reward function in (7). Table 1 presents the Monte Carlo results for $\alpha = \{0.1, 0.5, 0.9999\}$. In general, the α values do not significantly impact the overall performance. However, applying $\alpha = 0.1$ provides the best localization results in terms of estimation error and search duration. Applying $\alpha = 0.5$ proposed in (Ristic and Vo, 2010; Ristic et al., 2010) results in the worst performance, it increases flight time and travel distance necessary to complete the localization task. Using $\alpha = 0.9999$ (considered as using KL divergence which is a popular information gain measure) helps to save UAV travel distance while sacrificing location accuracy. One explanation for this scenario is that our noisy measurement causes the predicted posterior $p(\mathbf{x}_{k+H} | \mathbf{z}_{1:k}, \mathbf{z}_{k+1:k+H}^{(m)}(\mathbf{a}))$ in (7) to be less informative due to high uncertainty. Therefore, the reward function should place more emphasis on the current posterior instead by using a small α value or setting $\alpha \rightarrow 1$ to completely ignore the future posterior. This also explains the reason for the worst localization performance observed when $\alpha = 0.5$ (equally weighting the current and the future posterior).

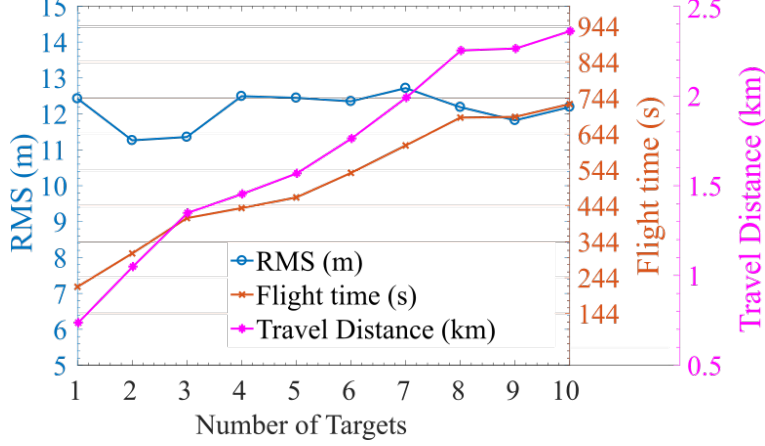


Figure 5: Localization performance for different number of targets N_{tg} increase from 1 to 10.

Second, we conducted experiments to understand how the action space set $N_{A,s}$ created by Alg. 1 affects our tracking performance in term of planning time and localization error. Table 2 shows Monte Carlo results for $N_{A,s} = \{2, 3, 4, 5, 6, 7\}$. Increasing the number of actions beyond four does not necessarily lead to better planning decisions because of the directionality of the antenna gain. Since the antenna gain is not omnidirectional, some actions result in changing the heading where antenna gain along the propagation path between the UAV and the target is lower; when the number of actions evaluated are increased, we encounter instances when an action leading to such a lower antenna gain in fact results in a higher reward. This result is a consequence of the inherent uncertainties in the models used in tracking and planning. Thus, we can see that $N_{A,s} = 4$ provides an adequate pool of actions to yield the best localization performance in terms of estimation error, flight duration and travel distance; a desirable result for realizing real time planning with limited computational resources.

Third, we want to examine the performance of our proposed algorithm under increasing number of targets; in this study we increase the maximum number of targets N_{tg} from 1 to 10. As depicted in the Fig. 5, our algorithm's estimation error was stable and invariant to the number of targets. Moreover, it is reasonable that the flight time and the travel distance increased linearly with target numbers because it took more time and power to track more targets.

Fourth, we examined the performance of the information gain measure, Rényi divergence, under different look-ahead horizons $H = N_{Htp}$ compared to: i) Shannon entropy (Cliff et al., 2015); ii) a naive approach that moves UAV to the closest estimated target location; and iii) a uniform search with predefined path used in (Ristic et al., 2010). Table 3 shows the Monte Carlo comparison results among various planning algorithms. All the parameters were reused

Table 1: Localization performance for different alpha values

	$\alpha = 0.1$	$\alpha = 0.5$	$\alpha = 0.9999$
RMS (m)	12.35	12.77	12.96
Flight time (s)	724	741	727
UAV travel distance (km)	2.38	2.41	2.34

Table 2: Localization performance for different number of actions

Number of actions $N_{A,s}$	2	3	4	5	6	7
RMS (m)	14.18	12.64	12.17	12.27	12.83	12.63
Flight time (s)	840	781	693	723	756	799
UAV travel distance (km)	2.62	2.53	2.39	2.50	2.52	2.70
Planning time (s)	1.16	1.19	1.23	1.27	1.36	1.47

Table 3: Localization performance for different planning algorithm

	Uniform	Closest Target	Shannon (Cliff et al., 2015)	Rényi			
N_H	N/A	N/A	1	1	3	5	10
t_p (s)	N/A	N/A	5	5	1	1	1
RMS (m)	18.8	13.4	12.6	12.5	12.4	12.0	11.6
Flight time (s)	921	799	774	699	889	811	822
UAV travel distance (km)	3.72	2.29	2.54	2.27	2.99	2.82	2.42
Planning Time (s)	1.58	1.11	1.38	1.28	1.53	1.65	2.71
Non-planning Time (s)	1.58	1.03	0.99	0.97	0.96	0.97	0.96

from the Sec. 5.1, except for $\alpha = 0.1$ and $N_{A,s} = 4$ were updated based on the previous experimental results. The result has demonstrated that Rényi divergence reward function is superior to other planning strategies in term of localization accuracy, including the Shannon entropy with the same horizon settings. For Rényi reward function itself, the large look ahead horizon number $N_H > 1$ helps to improve the localization accuracy; however, it requires higher computational power (planning) and causes the UAV to travel further. Using $N_H = 1$; $t_p = 5$ provides the best trade-off between computational time and accuracy.

Summary: According to the above simulation results, we select $\alpha = 0.1$, $N_{A,s} = 4$, and $N_H = 1$, $t_p = 5$ s as the planning parameters for the field experiment since these parameters provides the lowest computational cost, best performance in term of location estimation error, travel distance and flight time.

6 Field Experiments

We describe here our extensive experiments regime to validate our approach and evaluate the performance of our aerial robot system in the field. Our aim is to: *i*) investigate the possibility for signal interference from spinning motors of a UAV on RSSI measurements; *ii*) estimate the model parameters in the sensor model and validate the proposed model; and *iii*) conduct field trials to demonstrate and evaluate our system capabilities.

6.1 Rotors noise

We investigated the rotor noise to confirm that our system is not affected by the electromagnetic interference from the UAV’s motors. It also helps to clear the concern raised in (Cliff et al., 2015) that the rotor noise may affect the RSSI measurements. Four motors of the 3DR IRIS+ quad-copter shown in Fig.1 were used in this experiment. The RSSI data of a radio collar were measured across 149 MHz to 151 MHz frequency spectrum when four motors were operating at 20%, 50%, 100% of its maximum speed of 10, 212 rounds per minute. Fig 6 (a) shows the frequency spectrum of the received signal. We can see that there was no difference in the frequency characteristics when the rotors were in ON and OFF states. This result confirms that the rotors do not spin fast enough to generate high-frequency interference to impact our RSSI measurements.

6.2 Sensor model validation and parameter estimation

Antenna Gain: The antenna gain pattern was measured to verify its directivity compared to the antenna gain model $G_r(\mathbf{x}, \mathbf{u}) = G_r(\phi)$ calculated—following (Orfanidis, 2002, p.1252)—based on the physical design as discussed in Sec. 4. Fig. 6b shows the measured and modeled radiation patterns $G_r(\phi)$ in the E-plane. In the measurement process, ϕ is evaluated as the angle between the UAV heading, changed through 0° to 360° , and the direction from its position

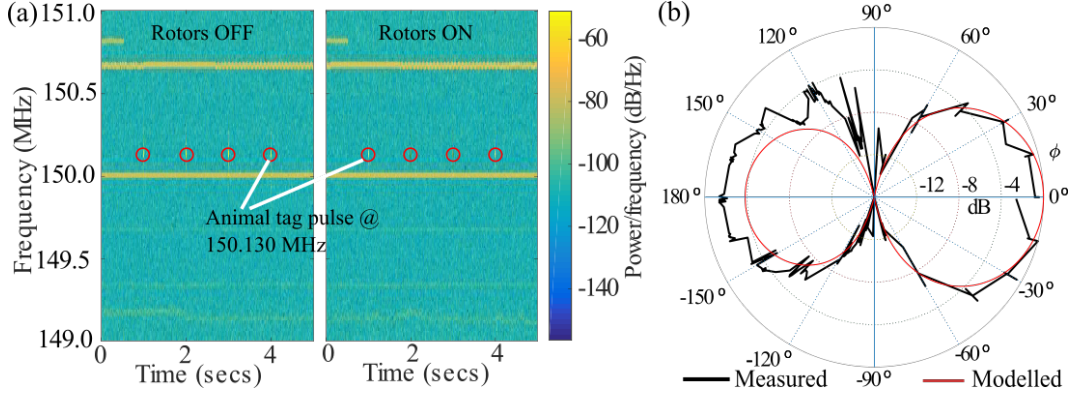


Figure 6: a) Waterfall plot for rotor noise experiment when four motors at full rotation speed; b) Normalized antenna gain in E-plane $G(\phi)$. The red line is gain modeled pattern and black line is the normalized measured gain pattern from 30 measurements collected by rotating the UAV heading at 15° intervals.

to a fixed location of a VHF radio tag. The result shows that the front-to-back ratio is smaller (2 dB) than expected and this is an artifact of folding the reflector on our design.

Signal propagation model parameter validation: We collected RSSI data points over a range from 10 m to 320 m between the UAV and a VHF radio tag. The tag and the UAV were kept at a height of 5 m above ground during this experiment. The tag was stationary at all times, while the UAV was directed to move away in a straight line from the tag at 10 m intervals whilst hovering at each location to allow the collection of approximately 30 measurements. The UAV heading was maintained to ensure consistent antenna gain during the experiment. Since we operated in an open terrain over a grassland, we selected the path loss exponent $n = 2$ suitable for modeling free space path loss. Fig. 7 shows the measured RSSI and the propagation models obtained using a nonlinear regression algorithm to estimate model parameters; we have the following results for reference power P_r^{d0} in (3), (4) at the reference distance $d_0 = 1$ m, and measurement noise variance σ_P in (5):

- **LogPath model :** $P_r^{d0} = -15.69$ (dBm) ; $\sigma_P = 4.21$ (dB).
- **MultiPath model :** $P_r^{d0} = -15.28$ (dBm) ; $\sigma_P = 2.31$ (dB).

The results show that both models, as expected, derived a similar reference power P_r^{d0} whilst providing a reasonable fit to measurement data and this affirms the validity of our propagation model. Although *LogPath* model is reasonable, *MultiPath* model is more accurate and yields a smaller measurement noise variance. The results confirm the impact of ground reflections, especially close to the signal source.

6.3 Field Trials

We present two sets of field experiments to validate the two measurement models and conducted a total of 16 autonomous flights to demonstrate our system capabilities. Our experiments were designed around University of Adelaide regulations governing the conduct of experimental UAV research. Given the need to operate in an autonomous mode, our flight zone, as well as the scope of the experiment, was restricted to University-owned property designated for UAV flight tests. Therefore: i) the UAV task was set to search and localize two mobile targets in a search area $75\text{ m} \times 300\text{ m}$ (2.25 Hectares); and ii) instead of wildlife, we relied on two people, each wore a VHF radio tag on their forearm, and a mobile phone-based GPS data logger on their hands to obtain ground truth; with two extra personnel stationed to maintain constant sight of the UAV as well a pilot in the field and abort the autonomous mode to transfer control to manual operations. The volunteers with the radio tags were asked to walk randomly and no other instructions were given.

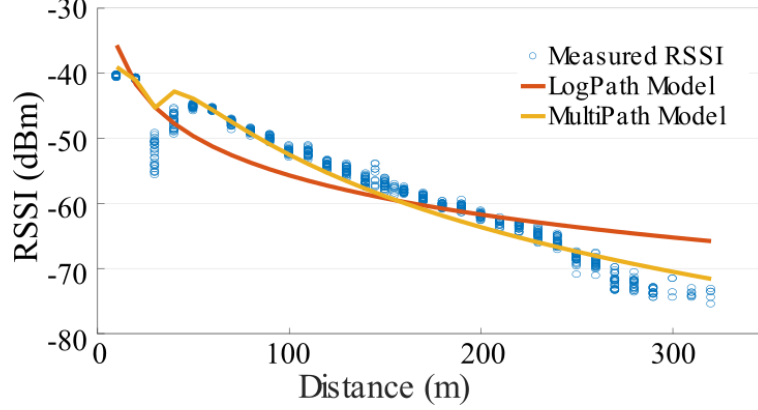


Figure 7: Plot of measured RSSI data points and its model estimates over a distance from 10 m to 320 m at 10 m intervals.

Fig. 8 shows the tracking and localization results along with UAV trajectories based on the two different measurement models. As expected, we observe the UAV planning has a tendency to approach the target's position since when the distance between the UAV and targets reduces, the RSSI measurement uncertainty is reduced. Thus it helps to reduce the uncertainty and increase the information gain. We can observe clear difference in the *LogPath* model and *MultiPath* model where UAV pursues the second target after completing the tracking task for target 1. The more accurate *MultiPath* model is able to track and localize the second target without needing a close approach. We can also observe that using *LogPath* model, where multipath propagation is not modeled but is clearly dominant close to the target, leads to a poorer localization accuracy despite the path planning algorithm leading the UAV close to the target.

Fig. 9 shows the particle distribution after the first observation is updated and when the targets are tracked and localized using the two measurement models. We can see that the solver is able to estimate the two tag positions quite accurately even after the update using the initial observation; however, the uncertainty (as noted by the particle distribution) is still very high. Interestingly, *MultiPath* model location uncertainty is significantly less where target 1 is placed in the bottom half of the field while target 2 is placed in the top half of the field. Target 1, being closer to the UAV, is localized first, with under 55 measurements for both measurement models. At the time when target 1 is localized, the uncertainty of target 2 is relatively higher for the *LogPath* model. The *MultiPath* model required significantly less measurements to track and localize target 2. As expected, both measurement models required significantly more measurements to localize the second target given the high measurement uncertainty associated with being much further than the first target from the UAV during its flight. Furthermore, random walk of the second target provided a challenging scenario since target 2 typically moved a larger distance around the field compared to the random walk performed by target 1.

Although the solver guides the UAV to move toward a target's position in both measurement models, as expected, the standard *LogPath* model is less accurate compared to the *MultiPath* model shown in Fig. 7; thus the uncertainty when using the *LogPath* model is higher and leads to longer time durations to localize the two tags. The consequence of model uncertainty resulting from the simple *LogPath* model, albeit still capable of locating both moving targets within the flight time capability of the UAV, is more apparent when the UAV makes an approach to the target and the distance to the target is less than 50 m depicted in Fig. 9c in comparison to Fig. 9f. We can see that the target location uncertainty increases for the *LogPath* model in the vicinity of 50 m and as a result the UAV requires an increasing number of maneuvers in its attempt to track and locate the target; this is clearly evident in the path followed for tracking and locating the second target. Table 4 presents the summary comparison results of location estimates between the two measurement models. Smaller RMS (root mean square) estimation error values suggest a higher accuracy, while shorter flight times and travel distance to localize all targets are highly desirable for a practicable system given the power constrained nature of commodity UAVs. The results confirm that the *MultiPath* model is superior to the standard *LogPath* model since it has been able to account for ground reflections and the UAV is not required to approach the target as closely when using the *LogPath* model to reduce its measurement uncertainty.

²Information regarding the total flight is not reported in (Cliff et al., 2015), however, as shown in Fig. 9 in (Cliff et al., 2015), one observation

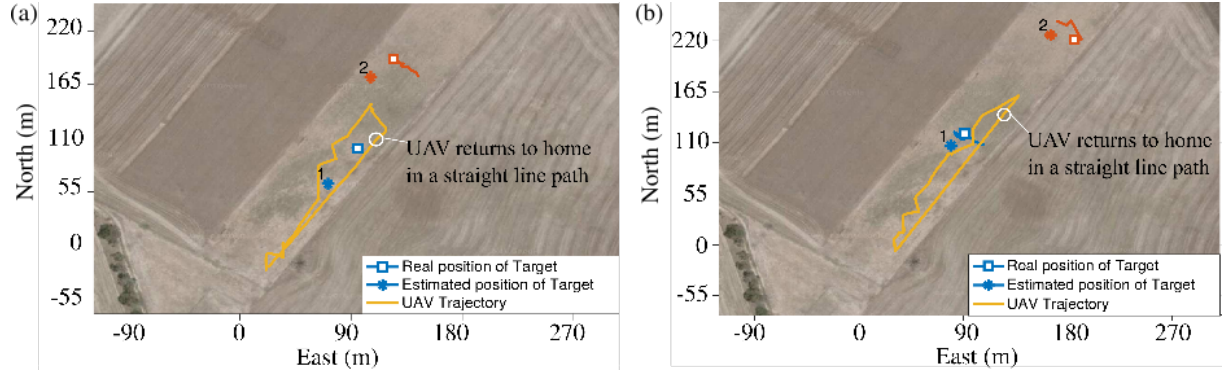


Figure 8: Field experiment results to search, track and localize two mobile tags for the two different measurement models. a) Standard **LogPath**. b) **MultiPath**.

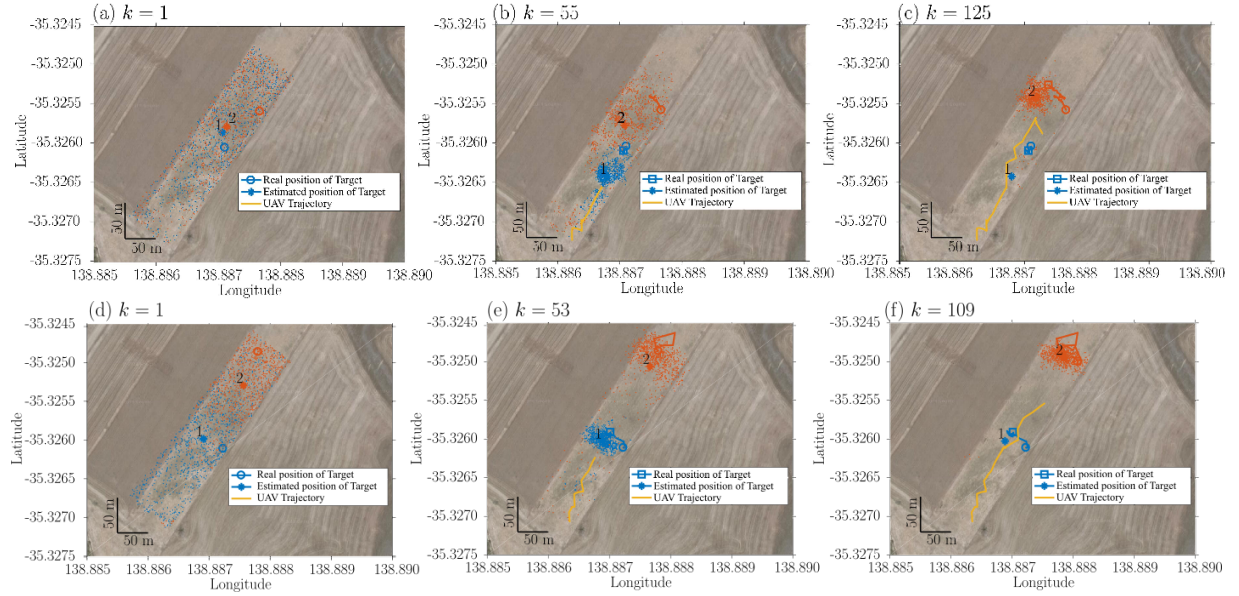


Figure 9: Field experiment results with the distribution of particles to search, track and localize two mobile tags. (a), (b) and (c) demonstrate the convergence of particles using the standard **LogPath** measurement model after the first observation is updated, the tag 1 is localized, and the tag 2 is localized, respectively. Similarly, (d), (e) and (f) demonstrate the convergence of particles using the **MultiPath** measurement model after the first observation is updated, the tag 1 is localized, and the tag 2 is localized, respectively. The blue and orange dots represent the start positions of the tag 1 and tag 2 respectively; the square symbols denote the ground truths of the localized tags; the star symbols denote the estimated positions of the tags; the solid yellow lines represent the UAV trajectories.

Table 4: Comparison of localization performance

Model	Target Type	Trials	RMS (m)	Total Flight Time (s)	Travel Distance (m)
LogPath	Mobile	8	30.1 ± 12.8	255 ± 104	549 ± 167
MultiPath	Mobile	8	22.7 ± 13.9	138 ± 53	286 ± 121
(Cliff et al., 2015)	Stationary	6	23.8 ± 14.0	838^2	N/A

Table 5: Comparison between our system and (Cliff et al., 2015) system.

	Ours	(Cliff et al., 2015)
<i>Payload (g)</i>	260	750
<i>Total mass (g)</i>	1,280	2,200
<i>Drone type</i>	Quadcopters (smaller drone)	Octocopters (relatively larger drone)
<i>Receiver Architecture</i>	Software defined radio (digital-based, rapidly scan multiple frequencies to support multiple frequencies)	Analog filtering circuit and a fixed frequency narrowband receiver (analog-based, difficult to re-configure for a new frequency)
<i>Antenna elements</i>	Compact, lightweight, folded 2-element Yagi antenna (designed for small drone form factor)	Antenna array structure requiring a large spatial separation of two antenna elements and wire ground plane
<i>Detection range (m)</i>	320	500
<i>Measurement model</i>	Range-only (exploiting the simplicity of a range-only measurement system)	Bearing-only (antenna array, and UAV rotation at grid points with a phase difference measurement system)
<i>Filtering method</i>	Particle filter ($O(N)$ operations per iteration)	Grid-based filter ($O(N^2)$ operations per iteration)
<i>Planning algorithm</i>	Rényi divergence	Shannon entropy
<i>Nature of targets</i>	Multiple mobile target tracking	A single stationary target localization

6.4 Discussion

In this section, we summarize results from our approach as well as compare and discuss our results in the context of the recent study by (Cliff et al., 2015). Table 4 presents a summary of localization field study results while Table 5 presents a complete comparison between our proposed system and (Cliff et al., 2015) system. Notably, our search area is smaller compared to (Cliff et al., 2015) ($75\text{ m} \times 300\text{ m}$ v.s $1000\text{ m} \times 1000\text{ m}$) due to our test flight zone restrictions, however, we have set up our initial distance from the UAV home position to its farthest target’s position (target #2 in this case) to be equivalent to the distance of the stationary target in (Cliff et al., 2015); approximately 300 m.

The results in Table 4 demonstrate that our proposed method can localize two mobile targets in a shorter flight time (the flight time of *MultiPath* model is one-sixth of that in (Cliff et al., 2015)) with better accuracy. Moreover, we search and locate two mobile targets; in contrast, (Cliff et al., 2015) method was implemented to locate a single and stationary target.

In general, as shown in Table 5, our system is more compact, lighter, and has a payload that is one-third of that in (Cliff et al., 2015) and consequently capable of longer flight times on any given UAV. Although our reliance on an SDR without a pre-amplifier has resulted in a shorter detection range, our total system mass being under 2 kg is significant since it enables ecologists to operate our system without a remote pilot licenses (RePL) (Civil Aviation Safety Authority, 2017). Moreover, the ability to instantly collect range-only measurements also helps reduce flight time significantly compared to the bearing-only method, requiring full rotations of a UAV at each observation point, as shown in the Table 4. Furthermore, as discussed in (Arulampalam et al., 2002), the computational cost for grid-based methods used in (Cliff et al., 2015) increases dramatically with the number of cells whilst the grid must be dense enough to achieve accurate estimations; *e.g.*, a grid-based filter with N cells conducts $O(N^2)$ operations per iteration, while a similar particle filter with N particles only requires $O(N)$ operations. Hence, the grid-based filter method only works in case of stationary targets as in (Cliff et al., 2015) where the most expensive computational step, the prediction step, is skipped. Moreover, as shown in Table. 3, our planning algorithm based on Rényi divergence is superior to the

took 76.21s and one trial needed 11 observations, hence total flight time is $11 \times 76.21 = 838.31\text{s}$

Shannon entropy approach in (Cliff et al., 2015) in terms of two important metrics: accuracy and UAV flight time.

7 Conclusion

We have developed and demonstrated an autonomous aerial vehicle system for range only tracking and localization of VHF radio-tagged animals under RSSI based measurement uncertainty and mobility of targets during their discovery in the field. The joint particle filter and POMDP with Rényi divergence based reward function provided an accurate method to explore, track and locate multiple animals while considering the resource constraints of the underlying UAV platform. In addition, we have realized a UAV system under 2 kg to ensure both the practicability and the accessibility of the technology to conservation biologists.

While we have demonstrated a successful system, we have only formulated our approach as a two-dimensional tracking problem that is ideally suitable for tracking endangered species in largely flat terrains and grasslands. Consequently, the current approach is not suitable for tracking wildlife in hills or mountainous areas and it would require: i) a UAV capability to maintain a fixed relative altitude above the ground; or ii) formulating a 3D tracking problem to extend our method to all topographical conditions. We leave the latter for future work.

Acknowledgments

This work was jointly supported by the Western Australia Parks and Wildlife (WA Parks), the Australian Research Council (LP160101177), the Defense Science and Technology Group (DSTG), and the University of Adelaide's Unmanned Research Aircraft Facility. We would like to thank the support and guidance provided by Mr. Adam Kilpatrick, Chief Remote Pilot and Maintenance Controller at the University of Adelaide, for making the field trials possible and and Remote Pilot, Mr. Fei Chen, Auto-ID Lab, The University of Adelaide for support provided in conducting all of the field experiments in the study.

References

- Arulampalam, M. S., Maskell, S., Gordon, N., and Clapp, T. (2002). A tutorial on particle filters for online nonlinear/non-Gaussian Bayesian tracking. *IEEE Transactions on signal processing*, 50(2):174–188.
- Beard, M. A., Vo, B.-T., Vo, B. N., and Arulampalam, S. (2017). Void probabilities and cauchy-schwarz divergence for generalized labeled multi-bernoulli models. *IEEE Transactions on Signal Processing*, 65.
- Civil Aviation Safety Authority (2017). AC 101-10 Remotely piloted aircraft systems - operation of excluded RPA (other than model aircraft). [Online; accessed 13-April-2018].
- Cliff, O. M., Fitch, R., Sukkariéh, S., Saunders, D., and Heinsohn, R. (2015). Online Localization of Radio-Tagged Wildlife with an Autonomous Aerial Robot System. In *Robotics: Science and Systems*.
- Gordon, N. J., Salmond, D. J., and Smith, A. F. (1993). Novel approach to nonlinear/non-Gaussian Bayesian state estimation. *IEE Proceedings F - Radar and Signal Processing*, 140(2):107–113.
- Hero, A. O., Kreucher, C. M., and Blatt, D. (2008). *Information theoretic approaches to sensor management*. Springer US.
- Hsu, D., Lee, W. S., and Rong, N. (2008). A point-based POMDP planner for target tracking. In *Proc. of IEEE ICRA*, pages 2644–2650.
- Jakes, W. C. (1974). *Microwave mobile communications*. Wiley, New York.
- Jensen, A. M., Geller, D. K., and Chen, Y. (2014). Monte Carlo simulation analysis of tagged fish radio tracking performance by swarming unmanned aerial vehicles in fractional order potential fields. *Journal of Intelligent & Robotic Systems*, 74(1-2):287–307.

- Kaelbling, L. P., Littman, M. L., and Cassandra, A. R. (1998). Planning and acting in partially observable stochastic domains. *Artificial Intelligence*, 101(1):99–134.
- Kays, R., Tilak, S., Crofoot, M., Fountain, T., Obando, D., Ortega, A., Kuemmeth, F., Mandel, J., Swenson, G., Lambert, T., et al. (2011). Tracking animal location and activity with an automated radio telemetry system in a tropical rainforest. *The Computer Journal*, pages 1931–1948.
- Körner, F., Speck, R., Göktogan, A. H., and Sukkarieh, S. (2010). Autonomous airborne wildlife tracking using radio signal strength. In *Proc. of IEEE/RSJ IROS*, pages 107–112.
- Orfanidis, S. J. (2002). *Electromagnetic waves and antennas*. Rutgers University New Brunswick, NJ.
- Ossmann, M. (2015). Software Defined Radio with HackRF.
- Patwari, N., Ash, J. N., Kyperountas, S., Hero, A. O., Moses, R. L., and Correal, N. S. (2005). Locating the nodes: cooperative localization in wireless sensor networks. *IEEE Signal processing magazine*, 22(4):54–69.
- Posch, A. and Sukkarieh, S. (2009). UAV based search for a radio tagged animal using particle filters. In *Australasian Conference on Robotics and Automation (ACRA)*, Sydney, Australia, Dec, pages 2–4.
- Ristic, B. (2013). *Particle Filters for Random Set Models*. Springer-Verlag New York.
- Ristic, B., Arulampalam, S., and Gordon, N. c. (2004). *Beyond the Kalman filter : particle filters for tracking applications*. Artech House.
- Ristic, B., Morelande, M., and Gunatilaka, A. (2010). Information driven search for point sources of gamma radiation. *Signal Processing*, 90(4):1225–1239.
- Ristic, B. and Vo, B.-N. (2010). Sensor control for multi-object state-space estimation using random finite sets . *Automatica*, 46(11):1812 – 1818.
- Silver, D. and Veness, J. (2010). Monte-Carlo planning in large POMDPs. In *Advances in neural information processing systems*, pages 2164–2172.
- Thomas, B., Holland, J. D., and Minot, E. O. (2012). Wildlife tracking technology options and cost considerations. *Wildlife Research*, 38(8):653–663.
- Tokekar, P., Bhadauria, D., Studenski, A., and Isler, V. (2010). A robotic system for monitoring carp in Minnesota lakes. *Journal of Field Robotics*, 27(6):779–789.
- Vander Hook, J., Tokekar, P., and Isler, V. (2014). Cautious Greedy Strategy for Bearing-only Active Localization: Analysis and Field Experiments. *Journal of Field Robotics*, 31(2):296–318.
- Wagle, N. and Frew, E. (2011). Spatio-temporal characterization of airborne radio frequency environments. In *IEEE GLOBECOM Workshops*, pages 1269–1273.
- Wikelski, M., Kays, R. W., Kasdin, N. J., Thorup, K., Smith, J. A., and Swenson, G. W. (2007). Going wild: what a global small-animal tracking system could do for experimental biologists. *Journal of Experimental Biology*, 210(2):181–186.